Multiple approaches for dosimetric characterization of a preclinical in vivo micro scanner: complementarity of experimental and numerical dose estimation

Alban Roussel, François Trompier, Bruno L'Homme, Karen Chaaya, Nathan Azemar, Yoann Ristic, Miray Razajanatovo, Gaëtan Gruel, Morgane Dos Santos

Multiple approaches for dosimetric characterization of a preclinical in vivo micro scanner: complementarity of experimental and numerical dose estimation

Alban Roussel[1], François Trompier[2], Bruno L'Homme[1], Karen Chaaya[1], Nathan Azemar[1], Yoann Ristic[2], Miray Razajanatovo[2], Gaëtan Gruel[3] and Morgane Dos Santos.[1*]

[1]*Autorité de sûreté nucléaire et de radioprotection (ASNR), PSE-SANTE/SERAMED/LRACC, F-92260, Fontenay-aux-Roses, France*

[2]*Autorité de sûreté nucléaire et de radioprotection (ASNR), PSE-SANTE/SDOS/LDRI, F-92260, Fontenay-aux-Roses, France*

[3]*Autorité de sûreté nucléaire et de radioprotection (ASNR), PSE-SANTE/SERAMED, F-92260, Fontenay-aux-Roses, France*

Purpose: The use of noninvasive imaging systems, such as microCT, is increasing for preclinical studies especially to perform longitudinal studies. Although this imaging system offers advantages, it relies on the use of low-energy X-rays, and the dose absorbed by the tissues during acquisitions must be considered. This study aims to estimate the absorbed dose to soft tissue and bone during mouse microCT imaging, using experimental and numerical methods.

Material and methods: Experimental measurements estimated the tissue dose in euthanized mice or mouse phantoms during acquisitions with a microCT (90 kVp). Doses were assessed using radiochromic films, an ionization chamber and alanine pellets. Absorbed dose in bone tissues was assessed through EPR spectroscopy using bone samples taken from mice. Monte Carlo simulations were performed with GEANT4 to compare with experimental data and obtain the 3D dose distribution.

Results: Experimental measurements for soft tissue dose estimation remains within acceptable limits, indicating satisfactory consistency between the different techniques of dosimetry (mean dose rate of 0.208 Gy/min ± 7.4% at the center of the abdominal mouse region), consistent with the manufacturer's estimation (0.228 Gy/min). Experimental and numerical methods show also good agreement for absorbed dose in bone, indicating that dose in bone is approximately seven times higher than that to tissue (relative difference between experimental and simulation values of 2.50%).

Conclusions: The complementarity of experimental and numerical methods allowed to accurately estimate dose deposition in soft and bone tissues. MicroCT acquisition can lead to significant dose deposition in animal tissues and should not be neglected.

Keywords: microCT; dosimetry; Monte Carlo simulation; radiobiology; soft tissue; bone

*corresponding author: morgane.dossantos@asnr.fr

Introduction

In recent years, numerous publications have highlighted the importance of dosimetry in radiobiology studies, emphasizing the need to accurately report irradiation conditions with a minimum level of detail and to describe the protocols used for dosimetric measurements (Marples 2020; DeWerd and Kunugi 2021). To improve dosimetry reporting, including the description of irradiation conditions and dosimetric parameters in publications, a lot of efforts have been led by European (Zoetelief et al. 1985; Stern et al. 2024) and American (Almond et al. 1999; Ma et al. 2001) working groups, leading to the publication of reference guidelines. In addition, more and more researchers are publishing the experimental protocols they have set up in their laboratories to help the scientific community in this process (Noblet et al. 2014; Dos Santos et al. 2018; Vaniqui et al. 2019; Tatu et al. 2020; Dos Santos et al. 2021; King et al. 2022; Bucher et al. 2022). While significant progress has been made and an increasing awareness of this issue can be observed in the literature, further efforts are still needed. This is underscored by the recent study by Draeger et al. (Draeger et al. 2020), which shows that many publications still overlook this aspect. To enhance practices in this field, recent articles have proposed guidelines, minimum reporting standards, and a checklist of key parameters that should be communicated (Poirier et al. 2023; Trompier et al. 2024; Stern et al. 2024). Additionally, they offer advice for researchers on how to accurately describe the dosimetry in their publications.

Beyond accurately characterizing the doses delivered during irradiations in radiobiological studies, it is also essential to assess the doses received by animals exposed to ionizing radiation as part of longitudinal monitoring via computed tomography (CT) imaging. Over the past few years, many clinical imaging techniques have been adapted for small animals, and the implementation of dedicated small-animal imaging systems in research laboratories has become widespread (Cunha et al. 2014; Lauber et al. 2017). These in vivo and non-invasive imaging systems are now essential for longitudinal studies, enabling the tracking of a pathology's progression over time in the same animal. Our laboratory has recently acquired a high-resolution small-animal CT imaging system, the Quantum GX2 (MicroCT Imaging | Revvity). This system allows CT imaging with or without contrast agents, analysis, quantification, and image fusion. It offers high resolution, fast imaging capabilities (few seconds to several minutes), and the possibility of respiratory or cardiac gating, covering a wide range of applications (pulmonary, cardiovascular, or bone microarchitecture research for example). While this imaging system has many advantages, it uses a low-voltage X-ray source (90 kVp), and the absorbed dose in the different tissues during acquisitions must be carefully considered. There are some concerns about the impact of repeated exposures and their associated dose deposition in tissues which could lead to bias in experimental results, especially for longitudinal studies. Therefore, accurately quantifying and interpreting imaging doses is essential in small-animal radiobiology research. Indeed, several publications have highlighted the impact of repeated CT scans on bone, resulting for example in decrease of trabecular bone volume (Klinck et al. 2008; Laperre et al. 2011). While some imaging systems deliver doses too low to cause measurable biological effects, other systems can deliver doses up to 1 Gy per scan, which may influence the results of longitudinal experiments. This issue is even more critical in radiobiology investigations focusing on low to moderate radiation doses, where the imaging dose can sometimes exceed the therapeutic dose. Additionally, for these low-energy X-rays, dose deposition occurs mainly through the photoelectric effect, which is highly dependent on the material's density (proportional to $(Z/E)^{3-5}$). The predominance of the photoelectric effect during dose deposition in dense materials such as bone leads to higher absorbed doses compared to soft tissues.

In the literature, it is possible to find a few publications dedicated to the dosimetric characterization of this type of equipment (Meganck and Liu 2017), but few of them have compared different experimental techniques or made direct comparisons between these experimental and numerical results. Moreover, many experimental studies use phantoms that do not accurately replicate the morphology of animals typically used in radiobiology research (Vrigneaud et al. 2013).

Thus, the objectives of this work were to characterize the absorbed dose in different tissues during CT image acquisition of mice at 90 kVp by conducting experimental dose measurements in soft and bone tissues, as well as Monte Carlo simulations. Experimental soft tissue dose measurements were carried out using three different methods (ionization chamber, radiochromic films and alanine pellets,

all calibrated in terms of absorbed dose to water). Absorbed dose in bone tissues was experimentally measured by Electron Paramagnetic Resonance (EPR) spectroscopy of bone. Given the low energies involved with microCT X-ray tubes, simulations allow to estimate the heterogeneities of dose deposition in soft and bone tissues and compare them to experimental results. Monte Carlo simulations allow for a highly accurate representation of the absorbed dose in different tissues and provide additional information about attenuation with 3D representation of deposited dose, which is not achievable experimentally. This multi-faceted approach, using complementary techniques, allowed us to accurately characterize dose deposition in various tissues and compare our results with those provided by the manufacturer. In the manuscript, the manufacturer's estimations refer to the nominal values provided by the manufacturer (doses expressed in Gy which depend on the acquisition parameters: Field Of View (FOV) and irradiation time) which also correspond to the values displayed on the microCT software interface during irradiation. This work allows also to better understand the actual dose delivered during acquisitions and optimize the number and frequency of CT images for longitudinal animal studies.

Material and methods

Installation characteristics

The Quantum GX2 (MicroCT Imaging | Revvity) is a high-resolution micro computed tomography (microCT) preclinical imaging system, specifically designed for small animals acquisitions such as mice and rats. Images are acquired using a computed tomography technique, based on a continuous rotation of an X-ray tube and detectors. The microCT is equipped with an X-ray tube with the following characteristics: 90 kVp voltage, 88 µA current, a tungsten anode with a 15° angle, an inherent filtration of 0.15 mm of beryllium and additional filtration composed of 0.50 mm of aluminum and 0.06 mm of copper. The distance from the exit window of the X-ray tube to the measurement point (at the center of the animal) is 3.5 cm. Two types of acquisitions were performed to estimate the dose rate: 4-minute (called "short" exposition) and 57-minute (called "long" exposition) acquisitions depending on the dosimeter used, with a 36 mm Field Of View (FOV), resulting in voxel size of 72 µm.

Experimental dosimetry

Estimating the dose absorbed by different tissues during a microCT acquisition required the use of mouse phantoms and euthanized mice. The phantoms are made from 'Mix D' (Brand et al. 1989), a tissue-equivalent material that can be molded when heated, and from a resin mold created using a euthanized mouse to achieve optimal anatomical accuracy. Mice used for irradiations were female C57BL/6J from Janviers Lab (Le Genest-Sait Isle, France), aged from 8 to 10 weeks. Experiments were performed in compliance with French and European regulations on protection of animals used for scientific purposes (French Decree 2013–118 and EC Directive 2010/63/EU), approved by the Ethics Committee 81 (approval number E92-032-01) and authorized by the French Ministry of (APAFIS#16160-2018071810588014 v2). Before performing dose measurements, mice were euthanized by cervical dislocation under gas anesthesia, in compliance with the regulations. The experimental estimation of absorbed dose to tissues was performed using different methods and dosimeters: ionization chamber, radiochromic films and EPR spectroscopy with alanine pellets for absorbed dose in soft tissue and absorbed dose in bone tissues by EPR on mouse's tibias. EPR spectroscopy is the only method able to determine experimentally the absorbed dose in bones by measuring the quantity of free radicals induced by irradiation in bones. For this study, two mice were used for ionization chamber measurements and eight mice were used for EPR measurements (soft tissue and bone dose estimations).

Ionization chamber

The ionization chamber used is the PTW 31002 (cylindrical, 0.125 cm^3 sensitive volume (PTW)) calibrated by an accredited laboratory in terms of absorbed dose in water (D_w). The detector was inserted into a euthanized mouse in the abdominal region, 5 acquisitions of 4 minutes and 3 acquisitions of 57 minutes were then performed to estimate the absorbed dose (in Gy). As recommended by reference protocols (Ma et al. 2001), measurements were corrected by the warm-up effect and correction factors (k_{pol}, k_{elec}, $k_{T,P}$). Then, the dose rate was determined for each configuration by dividing the measured

absorbed dose by the corresponding acquisition time (in $Gy.min^{-1}$). The overall uncertainty for measurements made with the ionization chamber is 3% at a 95% confidence level (k=2) including the uncertainty of the calibration factor, the measurements and correction factors.

Radiochromic films

Gafchromic EBT3 films from Ashland (Ashland 2023) were used. Calibration of radiochromic films could not be performed using the microCT due to technical constraints (inability to control irradiation times beyond the preset options) and geometrical limitations (restricted space). Therefore, calibration was performed with a low-energy X-ray installation dedicated to preclinical irradiation, the SARRP (Small Animal Radiation Therapy Platform, Xstrahl Ltd.), at 90 kVp, 20 mA, 1.5 $Gy.min^{-1}$, with same copper and aluminum filtrations as microCT. On this platform, comprehensive quality assurance procedures, including daily, weekly, and monthly checks, are implemented to ensure consistent performance, maintain system reliability, and enable early identification of operational deviations. The calibration curve was constructed using three films for each dose point, each irradiated individually in D_w (0.00 Gy, 0.25 Gy, 0.50 Gy, 0.75 Gy, 1.00 Gy, 1.50 Gy, 2.00 Gy, 3.00 Gy). Each film was 30 x 30 mm^2 in size. To avoid inter-film variation, three films were cut from the same EBT3 sheet and exposed to microCT X-rays. Each film, measuring 80 x 35 mm^2, was placed between the two parts of a mouse phantom with ultrasound gel to minimize air gaps, then the phantom was exposed to a 4-minute acquisition. The exposed zone to ionizing radiations on the film correspond to an area of 25 x 35 mm^2 centered on the middle of the phantom. Films used for calibration and films used for exposure to microCT X-rays were scanned on the same day using the Epson Perfection V700 scanner (EPSON 2023), following the protocol described by Dos Santos et al. (Dos Santos et al. 2021). The red channel method was employed for analysis, consisting of collecting the red pixel mean value, without background subtraction. Optical densities were then calculated and associated to irradiation doses to construct the calibration curve. The calibration curve is a fifth-degree polynomial curve, fitted to the mean values of each dose point using the polyfit function from NumPy python package (Array programming with NumPy | Nature). The equation of this curve was used to convert the optical densities of films irradiated using the microCT into absorbed dose. The mean absorbed dose value was studied on a large Region Of Interest (ROI) of 20 x 22 mm^2 in the center of the phantom and, on the other hand, several dose profiles were plotted to study the dose deposition inside the phantom. Uncertainties in dosimetric measurements using films arise from several sources: film calibration, absolute dose measurement with the ionization chamber, warm up and reproducibility of the scanner, measurement of the optical density. The maximum uncertainty is about 4% at a 95% confidence level (k=2).

EPR spectroscopy

EPR spectroscopy (Eaton et al. 2010) was used to evaluate the absorbed dose in both soft and bone tissues. This method consists of measuring the quantity of radio-induced free radicals (RIFRs), which is proportional to the absorbed dose in the sample. The EPR signal shape depends on the type of free radicals (FRs) present in the sample. The EPR signal intensity for a given type of RIFR is proportional to the quantity of the RIFR present in the material.

Soft tissue dose estimation: Alanine pellets are well-known tissue-equivalent dosimeters (Regulla and Deffner 1982). Their density differs slightly from that of soft tissue but their elemental composition (C, H, O, N) and effective atomic number ($Z_{eff} \approx 7.3$ for alanine vs. $Z_{eff} \approx 7.4$ for soft tissue) are highly similar, leading to comparable radiological interactions. For photons below 100 keV, however, an energy-dependence correction factor is required (Anton and Büermann 2015; Nasreddine et al. 2021). When a calibration curve is established in the same beam quality and setup (kVp, filtration, HVL, geometry), the energy dependence of alanine at low photon energies is inherently accounted for. Therefore, to ensure accurate dose measurements in our experimental conditions, we generated a dedicated calibration curve on the SARRP using the same beam quality as the microCT. In this work, we used in two sizes for this study: a “large” one (5 mm in diameter and 3 mm thick, mass of 65.5 ± 0.5 mg, density of 1.14 $g.cm^{-3}$, from Gamma-Service Medical GmbH) and a “small” one (4 mm in diameter and 2 mm thick, mass of 36.15 ± 0.06 mg, density of 1.247 $g.cm^{-3}$, from Aérial CRT). The small pellets were used to minimize potential attenuation effect within the dosimeter, given the low energies of the X-rays. For each size, the same batch of pellets was used, and a calibration curve was constructed in

terms of D_w with pellets irradiated in the SARRP installation. The alanine pellets were placed at 35 cm from the source at 1 cm depth in a water-like solid phantom with a total dimension of 20 x 20 x 6 cm^3 (Gammex Inc). A single irradiation was performed for each pellet and 3 pellets were irradiated for each dose point (4 Gy (only for large pellets), 8 Gy, 12 Gy, 16 Gy and 20 Gy). Then, 8 euthanized mice were used for microCT acquisitions, 4 for each pellet size. Alanine pellets were wrapped with Parafilm for waterproofing and placed inside the abdomen of each mouse, then exposed to the longest acquisition of 57 minutes to maximize the dose deposition and ease EPR measurements. This corresponds to eight distinct alanine pellets, each used for a different mouse to obtain a single measurement of the soft tissue dose. The alanine pellets were read out after a minimum delay of 14 days after irradiation to ensure the full stabilization of RIFR. The large pellets were measured using a benchtop X-band EPR spectrometer (Magnettech ESR5000), while the small pellets were measured using a Bruker X-band ELEXSYS E500 spectrometer (Bruker 2023). Alanine pellets irradiated for calibration and dose estimation in mice were measured on the same day, at a room temperature maintained to 19 °C. Each pellet was read at least four times to have a relative standard deviation of measurements consistently below 5%. Calibration curves were used to determine the absorbed dose in alanine pellets irradiated by the microCT. These curves are described by linear regressions, calculated using the linregress function from the Python scipy.stats package (Virtanen et al. 2020). All measurement points were used to determine the linear regression. Uncertainties on doses of pellets irradiated with microCT were calculated with the simplified propagation of uncertainty formula, which depends on the mean value and standard deviation of the series of independent EPR measurements, and the coefficients of the calibration curves and their associated uncertainties (given by linregress). Table 1 summarizes the acquisition parameters for small and large alanine pellets.

Table 1. Acquisition parameters of small and large alanine pellets used for soft tissue dose estimation.

Pellet size	**Small**	**Large**
Spectrometer used	ELEXSYS E500 (X-band)	ESR 5000 (X-band)
Number of readings	4	
Number of scans per reading	1	5
Duration of a scan (seconds)	60	60
Magnetic field range (mT)	326 – 346	344.5 – 357.5
Attenuation (dB)	10	20
Microwave power (mW)	10	2
Modulation (mT)	0.7	0.5
Room temperature (°C)	19	

Finally, the mean absorbed dose by an alanine pellet is estimated using a bootstrap method. This approach consists in simulating many samples (10^7 for our values), with each measurement represented by a normal distribution characterized by its central value and uncertainty. By analyzing the distribution of the mean values calculated on these samples, a global mean value and uncertainty (standard deviation) are determined.

Bone dose estimation: To study the dose deposition in bone during a microCT acquisition, tibias from the 8 irradiated mice were collected. Tibias were cleaned of tissues (skin, muscles, tendons, bone marrow), then dried and cut into small pieces for analysis. EPR measurements were performed at least 4 days after cutting to avoid unstable signals induced by mechanical stress. The X-band ELEXSYS E500 spectrometer was used bones measurements. Each bone was measured between 3 and 5 times, with 10 scans per measurement with a magnetic field sweep ranging from 348 mT to 353 mT, a microwave power of 3.991 mW and with a modulation amplitude of 0.5 mT. All measurements were performed at a room temperature of 19 °C. To avoid the effect of bone piece orientation on the results, their position and orientation were changed in the tube between each acquisition by shaking the samples pieces in the measurement tube. To determine the absorbed dose to the tibias, the additive dose method was employed (Journal of the ICRU 2019, Chapter 4: Electron Paramagnetic Resonance Dosimetry 2019), which

involves re-irradiating the tibias with known doses. Since the amplitude of the signal is proportional to the quantity of RIFR and, therefore, to the absorbed dose, re-irradiating the sample allows to construct a calibration curve specific to each bone sample. This approach is recommended for samples presenting a large inter-sample variability of their doe response, allowing a better accuracy than using a calibration curve even if more time consuming. These curves are linear regressions calculated using linregress, which provides the parameters a and b of the curves allowing the determination of the initial bone dose deposited after the irradiation. Re-irradiations were performed with a linear accelerator at 10 MV in term of air kerma (K_{air}) under electronic equilibrium conditions (Dair≈Kair). For high energy photon, density of the materials do not drive the dose deposition process and the kerma in air is equivalent to the kerma in bone (ISO 13304-2:2020 standard (ISO 13304-2:2020, p. 13304–2)), therefore EPR signal can be related to the absorbed dose in bone. Tibias were re-irradiated all together with 5 additive doses (+40 Gy, +40 Gy, +100 Gy, +40 Gy and +40 Gy), and EPR measurements were performed at least 3 days after each re-irradiation to ensure stability of RIFR in samples. After each additive dose, bone samples were measured 3 times (5 times for the last additive dose) with the exact same conditions as previously mentioned. The uncertainty in the estimated dose is calculated using the simplified propagation of uncertainty formula, which depends on the mean value and standard deviation of the EPR measurements, as well as the coefficients of the calibration curve and its associated uncertainties (given by linregress). Finally, the average absorbed dose in a mouse tibia is calculated and its uncertainty corresponds to the standard deviation, reflecting the variability of doses between tibias.

During each re-irradiation of tibias, two alanine pellets were placed in the field to measure the delivered dose to the tibias, inside the same type of container as that used for bones. This was done to construct accurate additive dose curves for each tibia, using an actual measured dose instead of the prescribed dose in K_{air}. Therefore, a calibration curve for these alanine pellets was constructed in K_{air} with 10 MV X-ray (20 Gy, 40 Gy, 60 Gy, 80 Gy and 120 Gy), with two pellets per dose, one irradiation per pellet. Measurements of both calibration pellets and those used during additive dose irradiations were performed on the same day using the MS5000X benchtop spectrometer, with the same parameters and uncertainty calculations as those used for soft tissue dose estimation.

Finally, for each mouse, a D_{bone}/D_{tissue} ratio was calculated between the absorbed dose to the bone (determined by the mean absorbed dose to the tibias) and the absorbed dose to the soft tissue (determined by the absorbed dose to the alanine pellet). The uncertainty associated to each ratio was calculated using the propagation of uncertainties. This ratio gives an idea of how much more dose is absorbed by bones compared to soft tissues during a microCT acquisition of the pelvic area of a mouse and can be compared with the results of the Monte Carlo simulations.

Monte Carlo simulations

The study of dose deposition after microCT exposure was conducted numerically by Monte Carlo simulations to compare experimental results and manufacturer estimations. Simulations were performed using GEANT4 (version 11.01.p01), an open-source C++ code designed for modelling particle interactions with matter, covering energies from eV to TeV (Agostinelli et al. 2003). The Livermore Electromagnetic physics list was used for calculations, with energy cuts of 250 eV for photons and 10 eV for electrons. The geometry of the microCT was implemented using information provided by the manufacturer and measurements taken directly on the microCT. It involved creating volumes for the X-ray tube envelope, anode, filtration layers (aluminum, copper and beryllium), plexiglass support and protection between the support and the detector. All materials were taken from the GEANT4 material database.

A unique random seed was associated to each simulation run, then several runs were launched with a large number of photons by run to ensure convergence and to verify the stability of the results. The statistical uncertainty of the Monte Carlo simulations was evaluated through these repeated runs and is reflected in the uncertainties reported for the analyzed quantities.

Source model

To save computing time, a virtual source of the microCT was modelled and implemented. Therefore, the first part consisted of simulating the real source of electrons ($1.90x10^{11}$ electrons launched), while the second part focused on simulating the virtual source of photons ($2.40x10^{7}$ photons launched). Comparisons were then made between these two sources. First, the real source of 90 keV electrons was implemented as a circular beam with 7 µm radius (manufacturer information) and focused on the anode. X-rays generated by bremsstrahlung interaction of electrons with the anode were collected at the exit window. For each photon collected, its energy, position and direction were stored. These data allowed the modelling of the virtual source of photon, where the anode and filtrations were removed from the geometry. Photons were generated on a circle with a 7 µm radius positioned at the anode's surface position, within a cone entirely covering the exit window of the X-ray tube. Similarly, information on each photon from the simulations with the virtual source was collected at the exit window to be compared to the results obtained with the real source. Energy spectra obtained from simulations were compared to the 90 kVp spectrum generated by the SpekPy toolkit (Poludniowski et al. 2021) , as well as the mean energy. The uncertainties on mean energies obtained by simulation were calculated using the bootstrap method, which consists of creating many new datasets (2000) by randomly sampling with replacement from the original data. For each resampled dataset, the mean energy was calculated, generating a distribution of mean values. The standard deviation of this distribution was then used as the final estimate of the uncertainty on the mean energy, providing a reliable measure without assuming a specific underlying distribution.

Dose computation

Once geometry and source model were implemented, dose deposition was studied in two configurations.

First, to guarantee a homogeneous irradiation, several angles of incidence were tested and validated for the simulations (0, 45, 90, 135, 180, 225, 270 and 315 degrees), with the same number of particles for each one. For this evaluation, the distribution of dose deposition in a segmented version of the mouse phantom was studied (configuration 1). In this simplified volume, more than 8 million voxels of 144 μm^3 of water were used to model a part of the mouse phantom. This voxelized phantom was generated from CT images of a dosimetry phantom created from a cast of a real adult C57Bl/6J mouse, commonly used in our lab. This ensures that the phantom closely matches the morphology of the animals used in our experiments. Especially, the CT images used to generate the voxelized phantom correspond to those acquired during the irradiation of radiochromic films (see Experimental dosimetry, Radiochromic films section) to allow comparison with experimental results. After simulating irradiation (1.72×10^{8} photons launched distributed equally across the 8 angles), the deposited energy in each voxel was collected and normalized to the maximum value. Then, these results were represented in 3D using the plotly python package (Plotly Technologies Inc. 2015), with each voxel assigned a color based on the normalized dose value, which is proportional to the energy.

Then, to study the heterogeneity of dose deposition between tissues, especially soft and bone tissues, a simplified model of mouse was implemented using volumes from GEANT4 (configuration 2). Based on macroscopic observations and anatomical measurements on CT images, the pelvic area and paws were designed using ellipsoids, cylinders and cones. Bones such as tibias were also designed, as well as an alanine pellet positioned in the abdomen (small size), as it was done for experimental measurements. For each of the eight simulations, 4.00×10^{9} photons were simulated from the source at a single angulation, resulting in a total of 3.20×10^{10} photons to simulate a complete rotation of the X-ray tube around the phantom. The total energies deposited in these volumes were stored, and the mean absorbed doses were calculated using volumes and densities of the pellet and the tibias, then compared to the experimental results by calculating the D_{bone}/D_{tissue} ratio. The simulation was run eight times to have a mean value of the D_{bone}/D_{tissue} ratio and an uncertainty corresponding to the standard deviation between the eight values.

Results

Experimental dosimetry

Ionization chamber

The mean dose rate in the mouse calculated from the ionization chamber measurements are 0.208 ± 0.001 Gy.min^{-1} and 0.205 ± 0.001 Gy.min^{-1}, respectively for the 4-minute (5 measurements) and 57-minute (3 measurements) acquisitions, where the uncertainties correspond to the standard deviation SD. Therefore, the mean dose rate estimated with the ionization chamber is 0.207 ± 0.002 Gy.min^{-1} (SD) at a single point inside the abdomen of a euthanized mouse.

Radiochromic films

Figure 1 depicts the irradiation conditions of a radiochromic film inside the mouse phantom with the microCT (1.B) and the dose distribution at different points on these films (1.C), determined using the calibration curve (1.A).

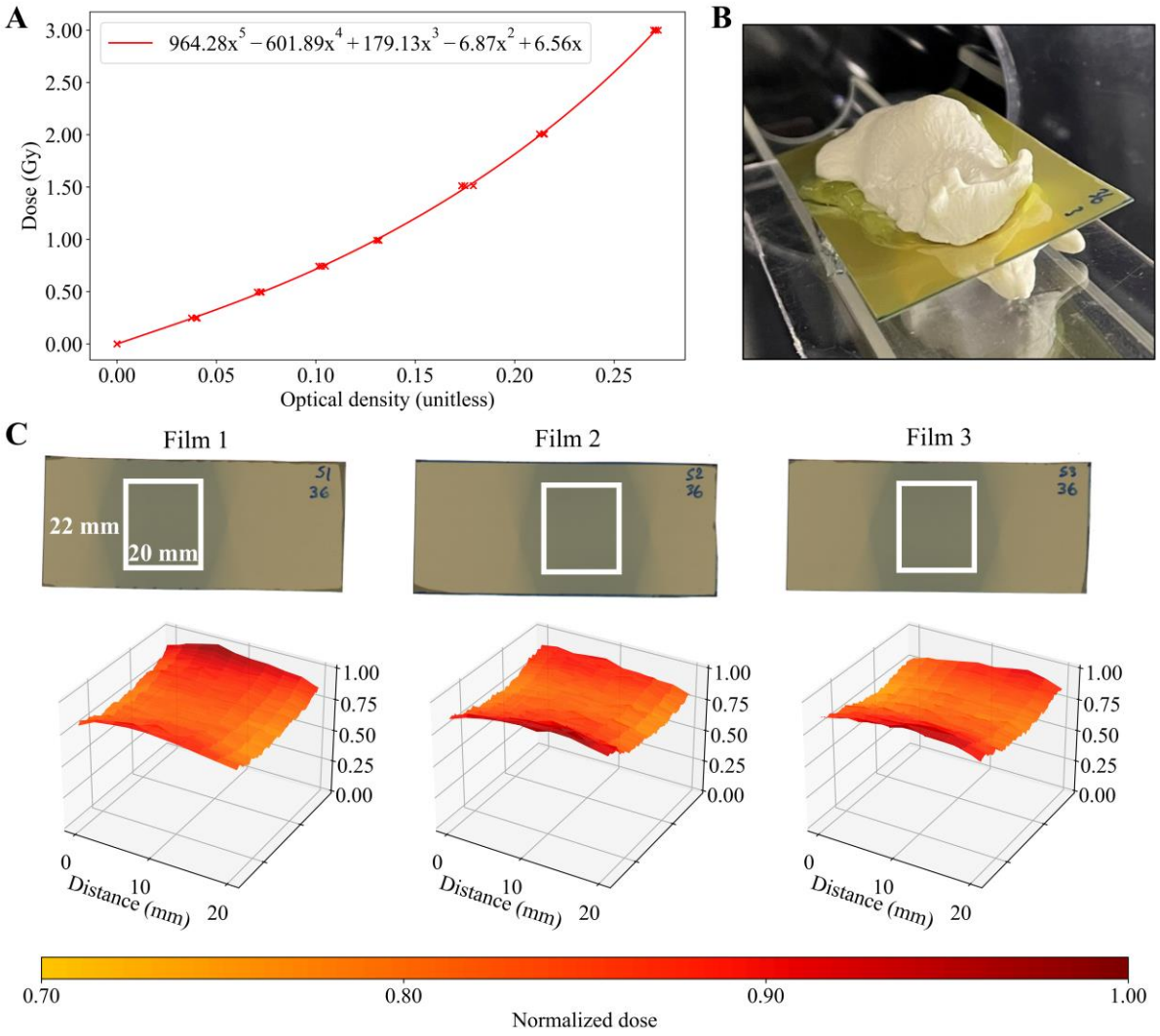

Figure 1. Use of EBT3 radiochromic films for tissue dose estimation. 1.A: Calibration curve of the radiochromic films, representing the dose (Gy in D_w) as a function of optical density (unitless). 1.B: Photograph of the mouse phantom on the microCT irradiation table, with a radiochromic film placed between the two parts of the phantom using ultrasound gel. 1.C: Images of the three films irradiated with the microCT and their corresponding dose distributions (normalized to the maximal dose)

constructed with a succession of dose profiles. Ten dose profiles were extracted along the 22-mm segment (in the direction of the segment), perpendicular to the 20-mm axis. White rectangles illustrate the areas where the mean absorbed doses were estimated.

The mean dose of the 4-minute acquisition between the three films was estimated to be 0.760 ± 0.004 Gy (SD), which means that the radiochromic films give an estimate of a mean dose rate of 0.190 ± 0.001 $Gy.min^{-1}$ (SD) at the center of the mouse phantom (area of 20 x 22 mm^2, illustrated by a white rectangle on each film on Figure 1.C). Then, for each film, ten dose profiles were plotted on the area along the 22-mm segment perpendicularly to the 20-mm axis. These results show an inhomogeneous dose deposition in the mouse phantom with variations of normalized dose (normalization to the maximum dose value) up to 26% in the central region compared to extremities, as illustrated on Figure 1.C. This means that the periphery of the phantom absorbs doses 26% higher than the center of the phantom.

EPR spectroscopy

Figure 2 presents typical EPR spectra for alanine (2.A), with red arrows indicating the measured EPR amplitude on the main EPR peak, and the calibration curves for both small and large alanine pellets (2.B). The amplitudes are normalized to the pellet mass for small pellets, and to both the pellet mass and the amplitude of the internal ruby sample of the MS5000X spectrometer for the large pellets.

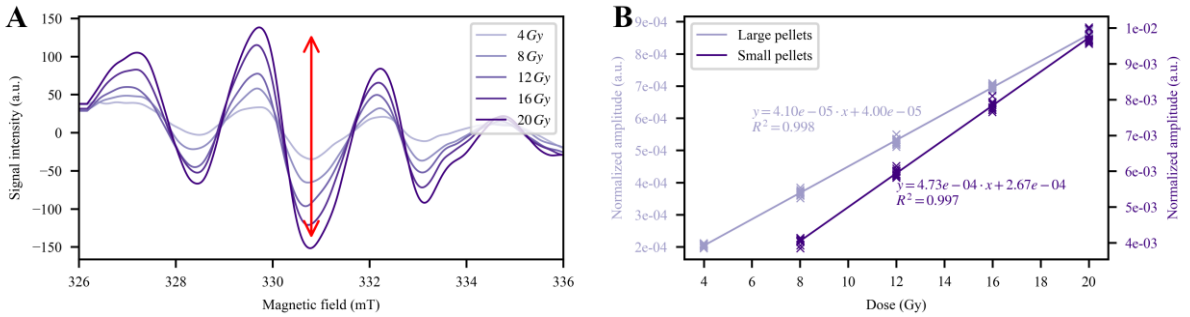

Figure 2. Use of alanine pellets for tissue dose estimation. 2.A: EPR spectra of the large alanine pellets irradiated to different doses used for calibration. The red arrow indicates the measured amplitude. 2.B: Calibration curves of small and large alanine pellets, showing the evolution of the normalized amplitude as a function of absorbed dose in the pellet.

Table 2 summarizes the absorbed doses by the alanine pellets during the 57-minute acquisition, determined using the curve equations from Figure 2.B.

Table 2. Absorbed doses by small and large alanine pellets during the long microCT acquisition and mean absorbed dose by pellet type. One alanine pellet was used per mouse and placed directly inside the abdominal cavity of the euthanized animal.

Pellet size	Mouse	Absorbed dose (Gy)	Mean absorbed dose (Gy)
Large	**1**	12.66 ± 0.26	13.23 ± 0.14
	2	13.60 ± 0.37	
	3	13.28 ± 0.16	
	4	13.39 ± 0.26	
Small	**5**	11.73 ± 0.22	11.60 ± 0.13
	6	12.05 ± 0.39	
	7	11.24 ± 0.18	
	8	11.38 ± 0.22	

The results show that the mean absorbed dose by the large alanine pellets is higher than the absorbed dose by that in the small pellets, with a difference of 1.63 Gy in the mean values. Therefore, the results of the large pellets indicate a dose rate of 0.232 ± 0.002 $Gy.min^{-1}$, whereas the small pellets indicate a dose rate of 0.203 ± 0.002 $Gy.min^{-1}$ (uncertainties on dose rates estimated using a bootstrap method with 10^7 samples) in the mouse.

Table 3 summarizes the experimental results for soft tissues, with for each dosimeter the subject of exposition (mouse or mouse phantom), the exposition type (short for 4 minutes or long for 57 minutes) and the mean dose rate (with standard deviation) in the subject. The two last columns provide the estimates of the manufacturer for both exposition types, provided without uncertainties.

Table 3. Mean dose rates in mouse soft tissue determined with different experimental methods (ionization chamber, EBT3 film, alanine pellet), in comparison with manufacturer estimations.

Dosimeter	**Ionization chamber**		**EBT3 film**	**Alanine pellet (small)**	**Alanine pellet (large)**	**Manufacturer**	
Subject	Mouse		Mouse phantom	Mouse	Mouse	?	
Exposition type	Short	Long	Short	Long	Long	Short	Long
Mean dose rate ($Gy.min^{-1}$)	0.208 ± 0.001	0.205 ± 0.001	0.190 ± 0.001	0.203 ± 0.006	0.232 ± 0.007	0.232	0.223

The experimental measurements carried out with the ionization chamber and the small alanine pellets closely matched. A slightly higher discrepancy was observed with large alanine pellets and radiochromic films, but the results are consistent with the other dosimeters. Considering all these experimental results, the mean dose rate in soft tissue is 0.208 ± 0.001 $Gy.min^{-1}$ (uncertainty calculated with 10^7 bootstraps). Regarding the radiochomic film results, the mean dose rate was determined based on the mean absorbed dose at the center of the phantom on specific areas as illustrated on Figure 1.C; whereas other techniques estimate the dose rate on a single point. A satisfactory consistency was found between the experimental measurements carried out with four types of detectors, but significative differences were found with the manufacturer's estimations (10.3% and 8.1% respectively for short and long expositions with ionization chamber, 18.1%, 9.0% and -4.0% respectively for EBT3 films, small and large alanine pellets). The manufacturer's estimation gives a mean dose rate of 0.228 ± 0.006 $Gy.min^{-1}$ (SD) in the mouse, which is higher than the experimental results for soft tissue in a mouse model (difference of 0.020 Gy. min^{-1} on mean dose rates).

The second part of the experimental study is dedicated to the evaluation of the absorbed dose in bone. Table 4 summarizes the mean absorbed doses from the two alanine pellets placed in the field during the additive dose irradiations. The uncertainties correspond to the standard deviations. The first additive dose (AD_01) for mice 5 to 8 could not be determined due to experimental problems, therefore the theoretical dose of 40 Gy was used for the additive dose curves.

Table 4. Additive dose values (Gy), corresponding to the absorbed doses by the alanine pellets placed in the irradiation fields.

Mouse number	AD_01 (Gy)	AD_02 (Gy)	AD_03 (Gy)	AD_04 (Gy)	AD_05 (Gy)
1 to 4	40.96 ± 0.25	40.67 ± 0.04	102.29 ± 0.48	40.85 ± 0.15	40.87 ± 0.35
5 to 8	40	40.84 ± 0.39	102.79 ± 0.90	40.96 ± 0.25	40.67 ± 0.04

Figure 3 summarizes bone dose estimation results.

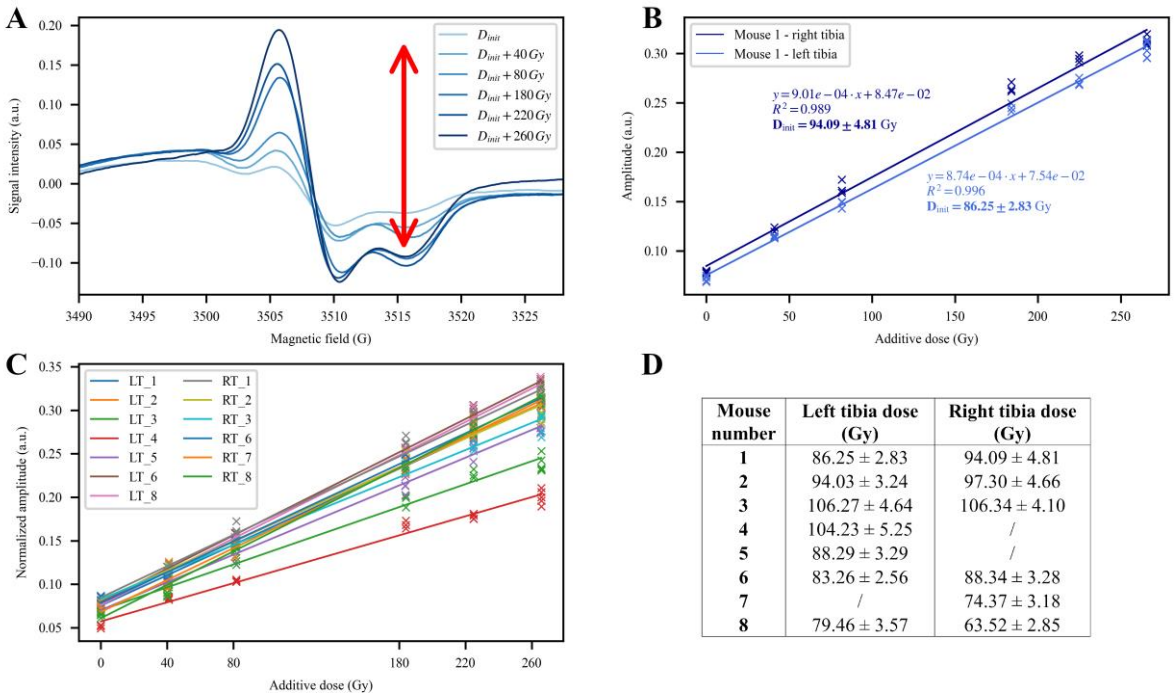

Mouse number	Left tibia dose (Gy)	Right tibia dose (Gy)
1	86.25 ± 2.83	94.09 ± 4.81
2	94.03 ± 3.24	97.30 ± 4.66
3	106.27 ± 4.64	106.34 ± 4.10
4	104.23 ± 5.25	/
5	88.29 ± 3.29	/
6	83.26 ± 2.56	88.34 ± 3.28
7	/	74.37 ± 3.18
8	79.46 ± 3.57	63.52 ± 2.85

Figure 3. Experimental results of bone dose estimation for an acquisition time of 57 minutes. 3.A: EPR spectra of an irradiated tibia after microCT exposition (D_{init}) and after re-irradiations of the additive dose method. The red arrow indicates the measured amplitude, proportional to the quantity of RIFR in the sample. 3.B: Additive dose curves of two tibias from the same irradiated mouse, representing the evolution of EPR signal amplitude (a.u.) as a function of the additive dose, and the derived D_{init}. 3.C: Additive dose curves of all irradiated tibias. 3.D: derived absorbed doses of irradiated tibias.

Figure 3.A shows different EPR spectra for a single tibia after the initial dose deposition due to microCT exposure (D_{init}) and after the additive doses. The red arrow shows the amplitude between the peaks which is proportional to the quantity of radio-induced free radicals in the bone and, therefore, to the absorbed dose. Figure 3.B presents the additive dose curves of both tibias from a mouse, obtained by measuring the amplitudes from the EPR spectra. From these curve parameters, initial doses absorbed by

the tibias were calculated to be 84.43 ± 2.78 Gy and 92.01 ± 4.70 Gy for left and right tibia respectively. This highlights the heterogeneity of absorbed dose between bone samples, even within the same animal.

Figure 3.C and Figure 3.D summarize the absorbed dose for all tibias during the 57-minute scans, derived from the additive dose curves. These results highlight the heterogeneity of additive dose curves, resulting in variable bone doses between animals (ranging from 63.52 Gy to 106.34 Gy, or 1.11 $Gy.min^{-1}$ to 1.87 $Gy.min^{-1}$ in dose rate terms) and sometimes between the two paws from the same one (difference of 15.95 Gy or 0.28 $Gy.min^{-1}$) between the tibias of mouse 8). Results from the table in Figure 3 allow estimating the mean absorbed dose in the tibia during a 57-minute acquisition to be 89.67 ± 12.72 Gy (SD), resulting in a dose rate in the bone of 1.57 ± 0.22 $Gy.min^{-1}$ (SD).

A ratio between the mean absorbed dose in the bones (both tibias) and the absorbed dose to the soft tissue (alanine pellet) was calculated for each mouse. These ratios are summarized in Table 5.

Table 5. Ratios between the mean absorbed dose to the bones and the mean absorbed dose to the soft tissue.

Mouse number	**1**	**2**	**3**	**4**	**5**	**6**	**7**	**8**
Ratio D_{bone}/D_{tissue} (unitless)	7.12 ± 0.26	7.03 ± 0.28	8.01 ± 0.25	7.78 ± 0.42	7.53 ± 0.31	7.12 ± 0.29	6.62 ± 0.30	6.28 ± 0.24

The mean ratio is 7.19 ± 0.11 (uncertainty calculated with 10^7 bootstraps), which means that experimental results indicate that bone absorbs around 7 times more dose than soft tissue during a microCT acquisition. This ratio between the dose to the bone and the dose to the tissue will be compared with the simulation results.

Monte Carlo simulations

Source model

To model the microCT, measurements were performed directly on the installation. Figure 4.A shows the interior of the microCT and especially the main elements such as the X-ray source, the filtrations, the mouse bed and the detector that were used to create the geometry. After modeling the geometry (Figure 4.B), simulations were run to collect the same number of photons (5.00×10^6 photons) at the exit window of the X-ray tube, using both the real source of electrons and the virtual source of photons.

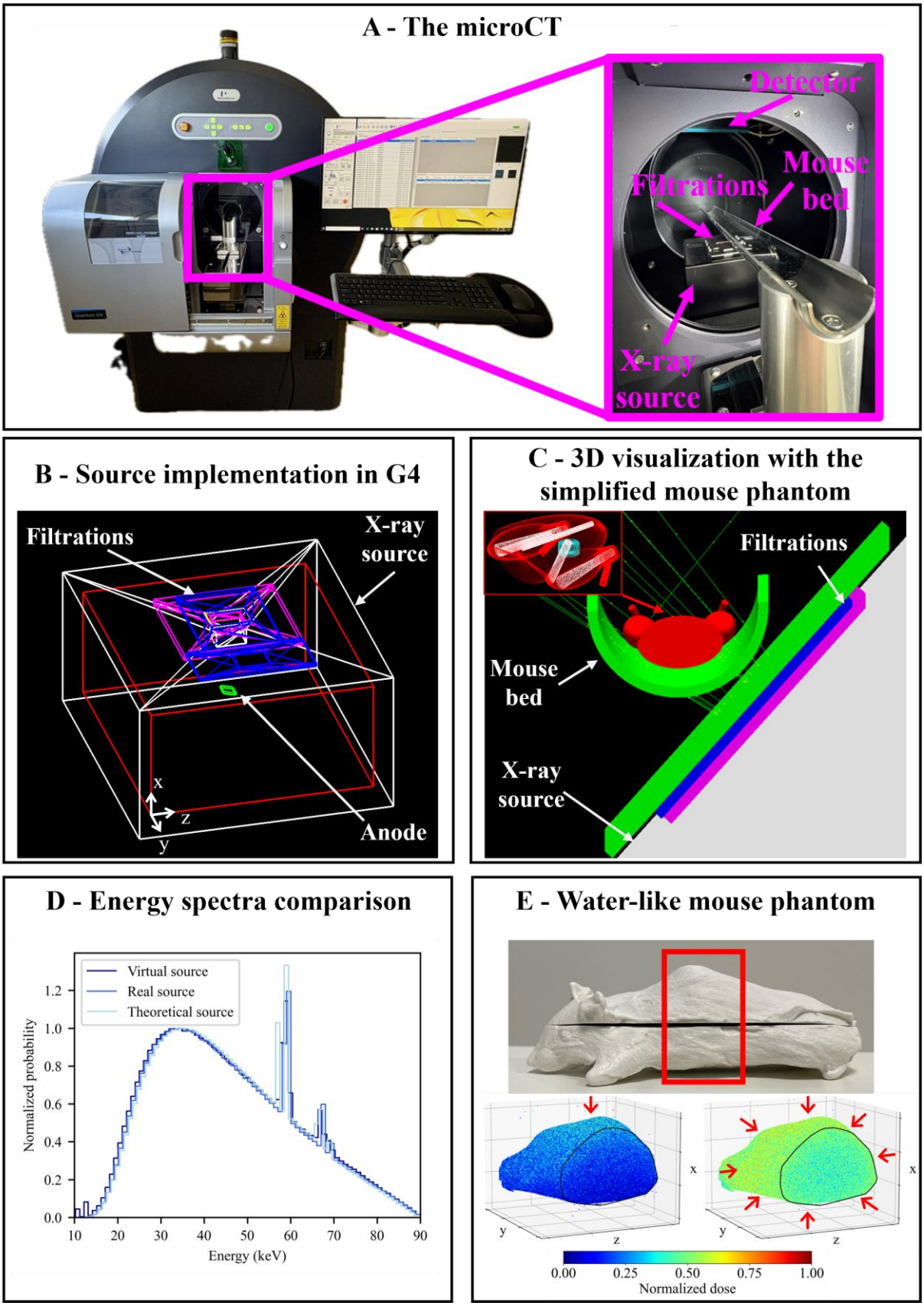

Figure 4. Simulation configurations using GEANT4. 4.A: Photograph of the microCT and zoom of its interior, showing the X-ray source, filtration elements, mouse bed, and detector. These components were measured for use in GEANT4 modeling. 4.B: Geometry of the microCT implemented in GEANT4 simulation (envelop with white, vacuum area with red, anode with green, support with pink, movable

support for filtrations with blue and filtrations with yellow). 4.C: Geometry of the simplified mouse model implemented in GEANT4 (configuration 2), where bones are shown in white, soft tissue in red, and the alanine pellet in cyan, along with a representation of the irradiation simulation at a 45-degree incidence, where green lines depict photon trajectories. 4.D: Energy spectra of the X-ray generated by the real source of electron, virtual source of photon and theoretical source from SpekPy (Poludniowski et al. 2021). 4.E: Water-equivalent mouse phantom used for experimental measurements with a red rectangle highlighting the segmented area used for simulations. The 3D representation of normalized dose in the water-like mouse phantom after simulations (configuration 1) with a single incidence (indicated by the red arrow) and the dose with all incidences is also depicted. The black line marks the front side of the phantom for clarity.

The energy of each photon was stored, and histograms (bins of 10 keV) were plotted on Figure 4.D to represent the energy spectra of the X-rays generated by these two sources, as well as the theoretical energy spectrum given by SpekPy (Poludniowski et al. 2021). The three spectra show good agreement in the shape, with slightly more intense characteristic rays of tungsten (KL, (Hudson 2003)) for the SpekPy spectrum. It results in a higher mean energy of the theoretical source (46.07 keV, no uncertainty provided), compared to the real and virtual sources (44.68 ± 0.01 keV and 44.53 ± 0.01 keV respectively).

Directions and positions of photons at the exit window were collected and analyzed (data not shown), revealing no significant differences in photon directions except along the z-axis, where the anode (heel) effect slightly shifts the angular distribution for the real source. The mean momentum difference along z is two orders of magnitude smaller than the natural spread of photon directions, corresponding to an extremely small variation in photon fluence and, consequently, a reduced impact on dose deposition. Moreover, photon positions at the exit window show a uniform irradiation field with both real and virtual sources. For these reasons, the anode effect is considered negligible for the simulations.

Dose computation

Figure 4.E illustrates the water-like mouse phantom used for experimental measurements with radiochromic films, where a red rectangle indicates the area segmented and implemented in GEANT4 for the configuration 1. Figure 4.E also shows dose deposition in the configuration 1 after irradiation at a single angulation (from above the phantom along the x-axis, illustrated with the red arrow) and after irradiation by the same number of photons at each beam angulation (along the arrows). These results highlight the necessity of choosing at least eight angulations to guarantee a homogenous irradiation, simulating a complete rotation of the X-ray tube around the phantom. The figure with all incidences shows dose variations inside the phantom up to 25%, with maximum doses at the outlines of the phantom, in agreement with the 26% obtained experimentally with radiochromic films.

Figure 4.C illustrates the simplified mouse phantom used in the configuration 2, representing the irradiation of this phantom at the angulation of 45 degrees. Based on the absorbed doses in the alanine pellet and the tibias, these results show that, on average, the tibias absorb 7.01 ± 0.01 times more dose than the alanine pellet. This factor is 7.62 ± 0.01 for the spinal column and 6.34 ± 0.01 for the femurs. Therefore, in the context of these simulations, the bones in the pelvic area of a mouse during a microCT acquisition absorb around 7 times more dose than soft tissues, represented by the alanine pellet as performed experimentally.

Discussion

Radiobiology aims to understand the mechanisms of biological effects of ionizing radiation. To achieve this, it is necessary to set safety standards for radiation. The importance of dosimetry for radiobiology studies is well established, and numerous publications highlight the need to detail irradiation conditions, describe the methodology employed and the dosimetric references used. To guide and support researchers, it is possible to find specific protocols in the literature, as well as guidelines and checklist of the minimum parameters that need to be reported (Poirier et al. 2023; Trompier et al. 2024; Stern et al. 2024). Although the situation is improving, it is still difficult to find all the information needed to reproduce experiments or understand all the physical parameters in the literature (Draeger et al. 2020). This is even more difficult when looking at CT imaging dosimetry data for preclinical studies. These imaging systems have developed considerably in recent years and have become essential tools for the longitudinal monitoring of animals. Although exposure times are generally limited (few minutes), the dose delivered by each acquisition must not be neglected, particularly when several scans are performed on the same animal over time. In addition, these imaging systems use low-energy X-ray sources, leading to very heterogeneous dose deposition due to the predominance of the photoelectric effect in these energy ranges. Very high doses can therefore be absorbed by dense tissues such as cortical bones (Chow et al. 2010; Chow and Jiang 2012; Guillou et al. 2022). The aim of this study was to characterize the dose delivered during acquisitions to the various tissues using experimental and numerical methods, and to compare the data with each other and with those supplied by the manufacturer to take this dose into account in our studies and optimize the frequency of acquisitions for long-term monitoring.

To carry out this study, we also used a SARRP installation to mimic the irradiation conditions of the microCT and to calibrate some of our detectors (EBT3 films and alanine pellets), as the geometry of the microCT system does not provide suitable conditions for performing this type of dosimetric measurement. In particular, the same additional copper and aluminium filtrations were applied on both platforms, but the inherent beryllium filtration (0.80 mm Be for the SARRP, 0.15 mm Be for the microCT) could not be modified. This difference in beryllium thickness results in a slight difference in Half-Value Layer (HVL) of 0.0004 mm Cu (calculated using the SpekPy tool (Poludniowski et al. 2021)). The resulting variation in beam quality was considered to have a negligible impact on the radiochromic film response, justifying the use of the SARRP for calibration.

Four dosimetry techniques were used to estimate the soft tissue dose. This approach enabled us to cross-validate the results, thereby ensuring greater accuracy. As each technique has its own uncertainties and biases, combining several methods reduces systematic errors and improves the accuracy of the estimates. Experimental measurements (Table 3) give a mean dose rate in soft tissue of 0.208 ± 0.001 Gy.min^{-1}. The different methods employed (ionization chamber, EBT3 radiochromic film, alanine pellets) remains within acceptable limits, indicating satisfactory consistency except for the large alanine pellet for which a higher dose rate in the mouse was measured. However, significant differences were observed with the manufacturer estimations (10.3% and 8.1% respectively for short and long expositions with ionization chamber, 18.1%, 9.0% and -4.0% respectively for EBT3 films, small and large alanine pellets).

The ionization chamber is the most straightforward and widely accepted method for dosimetry in preclinical research (International Atomic Energy Agency (IAEA) 2024). It has the advantage of providing the dose rate in real time and is known to have low dependence on energy, dose and dose rate. However, it has a non-negligible active volume (0.125 cm^3) compared to the size of the animals, is invasive and is difficult to set up due to the microCT geometry.

Another method to obtain the dose at a specific location is the use of alanine pellets. Alanine pellets have the advantage of being tissue-equivalent dosimeters with small dimensions, making them suitable for this study where they were placed directly inside the abdomen of animals. EPR spectroscopy employed for analysis of alanine pellets is a technique that provides accurate dose measurements with low uncertainties, especially in the high dose range. Two sizes of pellets were studied, resulting in a much significant difference in dose rate in the mouse compared to the experimental mean value for the large pellet (-11.8%) than for the small pellet (2.2%). Given the low voltage of the X-ray tube used by the microCT, significant attenuation of the beam is expected inside the animal but also within the alanine

pellet. Therefore, even if the dosimeter is irradiated from every angle due to the rotation of the X-ray tube, the homogenous deposition of energy inside the pellet cannot be guaranteed, especially for the large size (5 mm in diameter and 3 mm thick), which is a prerequisite to obtain accurate results. The small size (4 mm in diameter and 2 mm thick) should be preferred to limit the impact of this effect on the results. Additionally, smaller dosimeters are more suitable for dosimetry in small animals such as mice. These first two techniques enabled us to estimate the dose at a specific point in the model, which is therefore dependent on the position of this point. To assess dose heterogeneity over a larger volume of the mouse, radiochromic films were used.

EBT3 films can also give another estimation of the dose rate in soft tissue but require the use of a homogenous phantom, without considering different densities of tissues during dose deposition. The mean dose rate on the central region of the film shows a relative difference of 8.5% with the experimental mean value. However, the main strength of EBT3 films is to give an idea of dose distribution inside the animal, showing that a measurement made at a position can vary from another position due to differences in the anatomy of the mouse (differences of normalized dose up to 26%). Therefore, if the objective is to estimate the mean absorbed dose rate during a microCT acquisition, the use of radiochromic films may not represent the most appropriate choice among available dosimeters.

Based on our results, the experimental measurements suggest that the manufacturer's estimations refer to the absorbed dose in mouse soft tissue. The manufacturer provides a table outlining the doses delivered per acquisition, which depends on the FOV and acquisition time. However, there is a lack of details regarding the methods and dosimetric quantities, which are crucial for understanding how these doses were estimated. For more accurate information, it is advisable to consult the review by Meganck and Liu (Meganck and Liu 2017). The measurements were conducted with an ionization chamber placed inside a PMMA tube with a diameter of either 20 mm or 32 mm to simulate a mouse or a rat. While this type of phantom is commonly used to establish dosimetric configurations for preclinical studies, it does not accurately represent the animals involved and fails to consider tissue heterogeneity. In recent years, sophisticated phantoms have been developed to more accurately reproduce the animal's morphology and incorporate tissue heterogeneities (Welch et al. 2017; Esplen et al. 2019; Wegner et al. 2023). The validation of these phantoms is mainly carried out for a single morphology and type of mouse, but it is possible to find studies that show, for example, the impact of physical parameters (filtration, voltage) or mouse morphology on absorbed doses in different tissues (Belley et al. 2014; Caravaca et al. 2022). Taking all these parameters into consideration therefore seems to be a very important factor. In our work, to enhance precision and reflect reality when estimating doses during acquisitions, we opted to use euthanized animals for this study. Although, the mice are from the same strain and batch and are the same age, this approach allows us to consider tissue heterogeneity when estimating doses and enables experimental measurement of bone doses. However, mice from other strains and ages can vary significantly in mass and volume, leading to differences in beam attenuation during exposure, and consequently in dose deposition. For example, differences are observed in the body weight curves of mice of the same sex but from different strains (C57Bl6/J vs J:NU) at the same age, with variations up to 6.7 grams at 8 weeks. Similarly, mice of the same sex and strain show variations of up to 10 grams depending on their age (Body Weight Information for B6 at the Jackson Laboratory; Body Weight Information for Outbred Nude (007850) at the Jackson Laboratory). These morphological differences have an impact on the dose absorbed by tissues. MicroCT imaging systems can also be used with other animals, such as rats, which are significantly more voluminous, resulting in completely different real dose values compared to the manufacturer's estimations. Indeed, ionization chamber measurements were carried out by placing the chamber inside a euthanized rat. Dose estimation was performed for different CT acquisitions by varying the time by acquisition and the distance to source, resulting in dose differences up to -22.5%. These measurements highlight that manufacturer's estimations depend only on the CT acquisition time and not on the animal's shape.

The other experimental part of the study is dedicated to the estimation of the absorbed dose in bone during microCT exposure. Most experimental studies have focused on estimating radiation doses in soft tissues (Willekens et al. 2010; Rodt et al. 2011), while relatively few have addressed dose estimations in denser tissues like bone (Guillou et al. 2022; Guillou et al. 2024). This is particularly important for this type of X-ray beams, where dose deposition can be highly variable. Indeed, given the

low energy of photons generated by the 90 kVp X-ray tube, a significant part of the dose deposition occurs through photoelectric effect leading to high doses in dense tissues, such as bone. This heterogeneity of dose deposition is demonstrated by EPR measurements of the absorbed dose by the tibias resulting in a mean dose of 89.67 ± 12.72 Gy for the long acquisition, whereas in soft tissue the mean dose is 13.23 ± 0.14 Gy and 11.60 ± 0.13 Gy (given respectively by large and small alanine pellets results). Results show an important variability in the bone doses between the animals (up to 43 Gy) but also between the tibias from the same mouse (up to 16 Gy). Such differences cannot be justified only by a variability in the placement of the paws during exposition, but they may be due to differences in bone composition, which can be determining for bone dose estimation at low energies because of the predominance of photoelectric effect and its dependence on the atomic number ($(Z/E)^{3-5}$).

Experimental values show that a mouse tibia absorbs, on average, 7 times more dose than soft tissue (represented by an alanine pellet) when exposed to a 90 kVp source from the microCT imaging system. A study conducted by Guillou et al. (Guillou et al. 2022) with an 80 kVp X-ray source in simple incidence on mouse paws resulted in a similar order of magnitude of this factor (6.5 ± 0.9). The impact of a low energy imaging system is therefore non-negligible regarding dose deposition in the context of longitudinal follow-up of animals, especially when dense tissues such as bones are studied.

In addition, Monte Carlo simulations were carried out to evaluate the dose distribution in different tissues. These two approaches are complementary because experimental measurements take account of real conditions and uncertainties associated with the detectors or irradiation facilities used, but only allow the dose to be measured at a single point (or surface for radiochromic films), whereas simulation allows a global approach to dose estimation. The combination of experimental measurements and Monte Carlo simulations improves the reliability of dose estimates.

First, dose deposition was studied in a homogeneous phantom made of water voxels. The purpose of this initial simulation was to verify that the selected number of angulations was adequate for simulating tube rotation and to compare the simulation results with measurements obtained using radiochromic films. Therefore, the voxelized phantom was generated using the CT images acquired during the irradiation of radiochromic film placed in the mouse phantom. After simulations, the variation of normalized dose in the voxelized phantom reached 25% (mean value calculated over the same 20 x 22 mm^2 area, for specific slices corresponding to the position of the radiochromic film in the experiment), in close agreement with the 26% measured experimentally using EBT3 films. The simulated part of the phantom corresponds to the thickest region (Figure 4.E), leading to lower doses at the center than at the outline (Figure 4.E) due to the X-ray attenuation being more important in these few centimeters of matter compared to the extremities. The good agreement between the experimental data and the simulation validates the model.

Then, the objective was to numerically estimate the dose to the bone. Even though the phantom used is simplified to save calculation time, we were able to compare the ratios between the dose in the bone (tibia) and the dose in the tissue (alanine pellet) using the two approaches, showing good agreement. Indeed, the ratio is 7.19 ± 0.11 experimentally and 7.01 ± 0.01 by simulation (relative difference between experimental and simulation values of 2.50%). If Monte Carlo simulation allows to relatively quickly estimate this ratio (a few days in our conditions), it does not consider the variability between animals and even between the paws of one mouse (no difference in normalized dose between the tibias), which is a significant difference from the experimental data. To fully exploit the advantages of Monte Carlo simulations, it would be beneficial to introduce a voxelized phantom into the calculations. This type of phantom enables more precise distributions and highlights heterogeneities within the same tissue (Chow et al. 2010; Guillou et al. 2022). Ideally, multiple voxelized phantom types, varying in dimensions and representing different rodent species, would help account for variations among animals, such as differences in age, strain, and sex. This simulation provides a useful approach to estimate the ratio in a simplified configuration but is quite far from the experimental reality and remains complementary to it. On the other hand, performing only experimental measurements is not reasonably achievable in terms of number of animals used, and requires the use of different dosimetric methods to accurately estimate the doses.

By combining experimental measurements with numerical dose estimations, we accurately determined the absorbed doses in various tissues. The dosimetric characterization of the microCT will improve the optimization of protocols, especially concerning the frequency and duration of the scans, knowing that repeated and long acquisitions can lead to significant absorbed doses in the tissues. This effect should not be neglected, particularly when studies concern follow-up of the same animals and/or bone areas imaged by the microCT.

Acknowledgment

The authors would like to thank the GSEA of ASNR for technical assistance, especially Romain Granger, Amandine Sache, and Delphine Denais-Lalième.

Declaration of interest

The authors report no conflict of interest. The authors alone are responsible for the content and writing of the paper.

Funding

The author(s) reported there is no funding associated with the work featured in this article.

References

Agostinelli S, Allison J, Amako K, Apostolakis J, Araujo H, Arce P, Asai M, Axen D, Banerjee S, Barrand G, et al. 2003. Geant4—a simulation toolkit. Nuclear Instruments and Methods in Physics Research Section A: Accelerators, Spectrometers, Detectors and Associated Equipment. 506(3):250–303. https://doi.org/10.1016/S0168-9002(03)01368-8

Almond PR, Biggs PJ, Coursey BM, Hanson WF, Huq MS, Nath R, Rogers DWO. 1999. AAPM's TG-51 protocol for clinical reference dosimetry of high-energy photon and electron beams. Medical Physics. 26(9):1847–1870. https://doi.org/10.1118/1.598691

Anton M, Büermann L. 2015. Relative response of the alanine dosimeter to medium energy x-rays. Phys Med Biol. 60(15):6113. https://doi.org/10.1088/0031-9155/60/15/6113

Array programming with NumPy | Nature. https://www.nature.com/articles/s41586-020-2649-2

Ashland. 2023. Gafchromic dosimetry media, type EBT-3 [Internet]. http://www.gafchromic.com/index.asp

Belley MD, Wang C, Nguyen G, Gunasingha R, Chao NJ, Chen BJ, Dewhirst MW, Yoshizumi TT. 2014. Toward an organ based dose prescription method for the improved accuracy of murine dose in orthovoltage x-ray irradiators. Medical Physics. 41(3):034101. https://doi.org/10.1118/1.4864237

Body Weight Information for B6 at the Jackson Laboratory. https://www.jax.org/jax-mice-and-services/strain-data-sheet-pages/body-weight-chart-000664

Body Weight Information for Outbred Nude (007850) at the Jackson Laboratory. https://www.jax.org/jax-mice-and-services/strain-data-sheet-pages/body-weight-chart-007850

Brand JW, Kuba RK, Braunreiter TC. 1989. An improved head-and-neck phantom for radiation dosimetry. Oral Surgery, Oral Medicine, Oral Pathology. 67(3):338–346. https://doi.org/10.1016/0030-4220(89)90367-8

Bruker. 2023. ELEXSYS-II E500 CW-EPR [Internet]. https://www.bruker.com/en/products-and-solutions/mr/epr-instruments/epr-research-instruments/Elexsys-II-E500-CW-EPR.html

Bucher M, Weiss T, Endesfelder D, Trompier F, Ristic Y, Kunert P, Schlattl H, Giussani A, Oestreicher U. 2022. Dose Variations Using an X-Ray Cabinet to Establish in vitro Dose-Response Curves for Biological Dosimetry Assays. Frontiers in Public Health. 10:903509. https://doi.org/10.3389/fpubh.2022.903509

Caravaca J, Peter R, Yang J, Gunther C, Antonio Camara Serrano J, Nostrand C, Steri V, Seo Y. 2022. Comparison and calibration of dose delivered by 137Cs and x-ray irradiators in mice. Phys Med Biol. 67(22):225017. https://doi.org/10.1088/1361-6560/ac9e88

Chow JCL, Jiang R. 2012. Bone and mucosal dosimetry in skin radiation therapy: a Monte Carlo study using kilovoltage photon and megavoltage electron beams. Phys Med Biol. 57(12):3885–3899. https://doi.org/10.1088/0031-9155/57/12/3885

Chow JCL, Leung MKK, Lindsay PE, Jaffray DA. 2010. Dosimetric variation due to the photon beam energy in the small-animal irradiation: A Monte Carlo study. Medical Physics. 37(10):5322–5329. https://doi.org/10.1118/1.3488979

Cunha L, Horvath I, Ferreira S, Lemos J, Costa P, Vieira D, Veres DS, Szigeti K, Summavielle T, Máthé D, Metello LF. 2014. Preclinical Imaging: an Essential Ally in Modern Biosciences. Molecular Diagnosis & Therapy. 18(2):153–173. https://doi.org/10.1007/s40291-013-0062-3

DeWerd LA, Kunugi K. 2021. Accurate Dosimetry for Radiobiology. International Journal of Radiation Oncology*Biology*Physics. 111(5):e75–e81. https://doi.org/10.1016/j.ijrobp.2021.09.002

Dos Santos M, Paget V, Ben Kacem M, Trompier F, Benadjaoud MA, François A, Guipaud O, Benderitter M, Milliat F. 2018. Importance of dosimetry protocol for cell irradiation on a low X-rays facility and consequences for the biological response. International Journal of Radiation Biology. 94(6):597–606. https://doi.org/10.1080/09553002.2018.1466205

Dos Santos M, Paget V, Trompier F, Gruel G, Milliat F. 2021. Dosimetry for Cell Irradiation using Orthovoltage (40-300 kV) X-Ray Facilities. J Vis Exp.(168). https://doi.org/10.3791/61645

Draeger E, Sawant A, Johnstone C, Koger B, Becker S, Vujaskovic Z, Jackson I-L, Poirier Y. 2020. A Dose of Reality: How 20 Years of Incomplete Physics and Dosimetry Reporting in Radiobiology Studies May Have Contributed to the Reproducibility Crisis. International Journal of Radiation Oncology*Biology*Physics. 106(2):243–252. https://doi.org/10.1016/j.ijrobp.2019.06.2545

Eaton GR, Eaton SS, Barr DP, Weber RT. 2010. Quantitative EPR [Internet]. Vienna: Springer. https://doi.org/10.1007/978-3-211-92948-3

EPSON. 2023. Epson Perfection V700 [Internet]. https://www.epson.fr/produits/scanners/consumer/epson-perfection-v700-photo/p/1744

Esplen N, Alyaqoub E, Bazalova-Carter M. 2019. Technical Note: Manufacturing of a realistic mouse phantom for dosimetry of radiobiology experiments. Medical Physics. 46(2):1030–1036. https://doi.org/10.1002/mp.13310

Guillou M, L'Homme B, Trompier F, Errabii A, Marcoux T, Gruel G, Prezado Y, Santos MD. 2024. Radiological injuries under low energy x-rays in mice depending on dose and protocol: comparative characterization of lesion severity and impact of the in vivo bone response on retrospective dose estimations. Phys Med Biol. 69(4):045035. https://doi.org/10.1088/1361-6560/ad1d69

Guillou M, L'Homme B, Trompier F, Gruel G, Prezado Y, Dos Santos M. 2022. Preclinical modeling of low energy X-rays radiological burn: Dosimetry study by monte carlo simulations and EPR spectroscopy. Frontiers in Physiology [Internet]. 13. https://doi.org/10.3389/fphys.2022.1075665

Hudson L. 2003. X-ray Transition Energies, NIST Standard Reference Database 128 [Internet]. https://doi.org/10.18434/T4859Z

International Atomic Energy Agency (IAEA). 2024. Technical Reports Series no. 398. Absorbed Dose Determination in External Beam Radiotherapy [Internet]. [place unknown]. https://doi.org/10.61092/iaea.ve7q-y94k

ISO 13304-2:2020. ISO [Internet]. https://www.iso.org/fr/standard/66891.html

Journal of the ICRU 2019, Chapter 4: Electron Paramagnetic Resonance Dosimetry. 2019. 19(1):46–68. https://doi.org/10.1177/1473669119893153

King EJ, Viscariello NN, DeWerd LA. 2022. Development of Standard X-Ray Beams for Calibration of Radiobiology Cabinet and Conformal Irradiators. Radiat Res. 197(2):113–121. https://doi.org/10.1667/RADE-21-00121.1

Klinck RJ, Campbell GM, Boyd SK. 2008. Radiation effects on bone architecture in mice and rats resulting from *in vivo* micro-computed tomography scanning. Medical Engineering & Physics. 30(7):888–895. https://doi.org/10.1016/j.medengphy.2007.11.004

Laperre K, Depypere M, van Gastel N, Torrekens S, Moermans K, Bogaerts R, Maes F, Carmeliet G. 2011. Development of micro-CT protocols for in vivo follow-up of mouse bone architecture without major radiation side effects. Bone. 49(4):613–622. https://doi.org/10.1016/j.bone.2011.06.031

Lauber DT, Fülöp A, Kovács T, Szigeti K, Máthé D, Szijártó A. 2017. State of the art in vivo imaging techniques for laboratory animals. Laboratory Animals. 51(5):465–478. https://doi.org/10.1177/0023677217695852

Ma C-M, Coffey CW, DeWerd LA, Liu C, Nath R, Seltzer SM, Seuntjens JP. 2001. AAPM protocol for 40–300 kV x-ray beam dosimetry in radiotherapy and radiobiology. Medical Physics. 28(6):868–893. https://doi.org/10.1118/1.1374247

Magnettech ESR5000. https://www.bruker.com/fr/products-and-solutions/mr/epr-instruments/magnettechesr5000.html

Marples B. 2020. The Need for Accurate Reporting of Dosimetric Conditions in Radiobiology Studies. International Journal of Radiation Oncology*Biology*Physics. 106(2):253–254. https://doi.org/10.1016/j.ijrobp.2019.10.025

Meganck JA, Liu B. 2017. Dosimetry in Micro-computed Tomography: a Review of the Measurement Methods, Impacts, and Characterization of the Quantum GX Imaging System. Mol Imaging Biol. 19(4):499–511. https://doi.org/10.1007/s11307-016-1026-x

MicroCT Imaging | Revvity. https://www.revvity.com/fr-en/category/microct-imaging

Nasreddine A, Kuntz F, El Bitar Z. 2021. Absorbed dose to water determination for kilo-voltage X-rays using alanine/EPR dosimetry systems. Radiation Physics and Chemistry. 180:108938. https://doi.org/10.1016/j.radphyschem.2020.108938

Noblet C, Chiavassa S, Paris F, Supiot S, Lisbona A, Delpon G. 2014. Underestimation of dose delivery in preclinical irradiation due to scattering conditions. Physica Medica. 30(1):63–68. https://doi.org/10.1016/j.ejmp.2013.03.001

Plotly Technologies Inc. 2015. Collaborative data science Publisher: Plotly Technologies Inc. [Internet]. https://plot.ly

Poirier Y, DeWerd LA, Trompier F, Santos MD, Sheng K, Kunugi K, Satyamitra MM, DiCarlo AL, Winters TA. 2023. Minimum Reporting Standards Should be Expected for Preclinical Radiobiology Irradiators and Dosimetry in the Published Literature. Radiation Research. 200(3):217–222. https://doi.org/10.1667/RADE-23-00119.1

Poludniowski G, Omar A, Bujila R, Andreo P. 2021. Technical Note: SpekPy v2.0—a software toolkit for modeling x-ray tube spectra. Medical Physics. 48(7):3630–3637. https://doi.org/10.1002/mp.14945

PTW. https://www.ptwdosimetry.com/en/

Regulla DF, Deffner U. 1982. Dosimetry by ESR spectroscopy of alanine. The International Journal of Applied Radiation and Isotopes. 33(11):1101–1114. https://doi.org/10.1016/0020-708X(82)90238-1

Rodt T, Luepke M, Boehm C, von Falck C, Stamm G, Borlak J, Seifert H, Galanski M. 2011. Phantom and cadaver measurements of dose and dose distribution in micro-CT of the chest in mice. Acta Radiol. 52(1):75–80. https://doi.org/10.1258/ar.2010.100059

Stern W, Alaei P, Berbeco R, DeWerd LA, Kamen J, MacKenzie C, Moros EG, Poirier Y, Potter CA, Schaue D, et al. 2024. Recommendations for harmonized reporting of radiation Dosimetry by adoption

of Compatibility in Irradiation Research Protocols Expert Roundtable (CIRPER). International Journal of Radiation Biology. 100(6):821–823. https://doi.org/10.1080/09553002.2024.2331130

Tatu SS, Lo BID, Cortez JJM, Ortillo MJT, Bautista GFM, Erojo MJV, Feliciano CP. 2020. Dosimetric characterization of an X-ray irradiator for use with cells. Radiation Physics and Chemistry. 176:109065. https://doi.org/10.1016/j.radphyschem.2020.109065

Trompier F, DeWerd LA, Poirier Y, Dos Santos M, Sheng K, Kunugi KA, Winters TA, DiCarlo AL, Satyamitra M. 2024. Minimum reporting standards should be expected for preclinical radiobiology irradiators and dosimetry in the published literature. International Journal of Radiation Biology. 100(1):1–6. https://doi.org/10.1080/09553002.2023.2250848

Vaniqui A, Walters BR, Fonseca GP, Verhaegen F. 2019. Dose to water versus dose to medium from cavity theory applied to small animal irradiation with kilovolt x-rays. Physics in Medicine & Biology. 64(16):165001. https://doi.org/10.1088/1361-6560/ab2db1

Virtanen P, Gommers R, Oliphant TE, Haberland M, Reddy T, Cournapeau D, Burovski E, Peterson P, Weckesser W, Bright J, et al. 2020. SciPy 1.0: fundamental algorithms for scientific computing in Python. Nat Methods. 17(3):261–272. https://doi.org/10.1038/s41592-019-0686-2

Vrigneaud J-M, Courteau A, Ranouil J, Morgand L, Raguin O, Walker P, Oudot A, Collin B, Brunotte F. 2013. Application of the optically stimulated luminescence (OSL) technique for mouse dosimetry in micro-CT imaging. Medical Physics. 40(12):122102. https://doi.org/10.1118/1.4829499

Wegner M, Frenzel T, Krause D, Gargioni E. 2023. Development and characterization of modular mouse phantoms for end-to-end testing and training in radiobiology experiments. Phys Med Biol. 68(8):085009. https://doi.org/10.1088/1361-6560/acc566

Welch D, Turner L, Speiser M, Randers-Pehrson G, Brenner DJ. 2017. Scattered Dose Calculations and Measurements in a Life-Like Mouse Phantom. rare. 187(4):433–442. https://doi.org/10.1667/RR004CC.1

Willekens I, Buls N, Lahoutte T, Baeyens L, Vanhove C, Caveliers V, Deklerck R, Bossuyt A, de Mey J. 2010. Evaluation of the radiation dose in micro-CT with optimization of the scan protocol. Contrast Media Mol Imaging. 5(4):201–207. https://doi.org/10.1002/cmmi.394

Zoetelief J, Broerse JJ, Davies RW. 1985. Protocol for X-ray dosimetry - EULEP: Contract No BIO-390-81 F. Luxembourg: Office for Official Publications of the European Communities.